Laser-induced excitation and ionization of a confined hydrogen atom in an exponential-cosine-screened Coulomb potential

Shalini Lumb,[1,*] Sonia Lumb,[2,†] and Vinod Prasad[3,‡]

[1]*Department of Physics, Maitreyi College, University of Delhi, New Delhi-110021, India*

[2]*Department of Physics and Electronics, Rajdhani College, University of Delhi, New Delhi-110015, India*

[3]*Department of Physics, Swami Shraddhanand College, University of Delhi, Delhi-110036, India*

(Received 18 July 2014; revised manuscript received 16 August 2014; published 8 September 2014)

The energy spectra of spherically confined hydrogen atom embedded in an exponential-cosine-screened Coulomb potential is worked out by using the Bernstein-polynomial method. The interaction of short laser pulses in the femtosecond range with the system is studied in detail. The effect of shape of laser pulse, confinement radius, Debye screening length as well as different laser parameters on the dynamics of the system has been explored and analyzed.

DOI: 10.1103/PhysRevA.90.032505 PACS number(s): 32.70.−n, 32.30.−r, 31.15.ve, 31.15.vj

I. INTRODUCTION

During last few years, extensive focus has been placed on atomic systems confined in different plasma environments; for example, atom in Debye, Debye-cosine plasma, etc. [1–11]. In addition, such confined systems interacting with external fields have also been explored in quite significant detail. The reason for such motivated studies is their applicability in many diverse, interdisciplinary branches of science. These studies have been a subject of interest in condensed matter physics, biophysics, astrophysics, and many other fields. It is well known that an atomic system placed in a high-density plasma shows physical properties different from a free atom. A number of calculations on the structural properties of confined atoms have been reported in literature [12–14].

As mentioned by Lin and Ho [15], most of the plasmas found in nature or in laboratories such as the solar chromosphere, ionosphere, magnetic confinement, fusion, etc. are classical plasmas. Atoms embedded in such weakly confined plasmas have been very well described by so-called Debye plasmas. However, with increases in plasma density, instead of Debye, the modified Debye–Hückel model is used, i.e., the exponential-cosine-screened Coulomb potential (ECSCP) [15–18].

In the present work, we study the dynamics of a hydrogen atom confined in a spherical box and immersed in a Debye-cosine plasma environment. Recently, there have been a few studies on the dynamics of short pulses (in the attosecond range) with atomic [19] and loosely confined atomic systems [20]. In this paper we investigate the photoexcitation and ionization of hydrogen atoms confined in a Debye-cosine plasma in the presence of short pulses. In order to make a more elaborate investigation of the short-pulse interaction with confined systems, we study the interaction of different-shaped pulses to find the effect of pulse shape. A change in pulse shape is directly related to the manner in which the system is imparted energy. The shape effect on the dynamics is seen to be quite interesting.

In addition to pulse shape, there are many parameters, viz., Debye screening length λ_D, confining radius r_0, along with pulse duration, pulse intensity, and pulse frequency, which affect the dynamics very strongly. We show and analyze the effect of all such parameters on photoexcitation and ionization of hydrogen atoms.

II. PROBLEM FORMULATION AND METHOD OF SOLUTION

The nonrelativistic Hamiltonian of a spherically confined hydrogen atom in a dense quantum plasma modelled by ECSCP is given by

$$H_0 = \left[-\frac{1}{2}\nabla^2 - \frac{1}{r}\cos\left(r/\lambda_D\right) e^{-r/\lambda_D} \right] + V_c\left(r\right), \quad (1)$$

where λ_D is the Debye screening length and $V_c(r)$ is the confinement potential given by

$$V_c\left(r\right) = \begin{cases} 0, & r < r_0 \\ \infty, & r \geqslant r_0, \end{cases} \quad (2)$$

with r_0 being the confinement radius. The energy spectrum and wave functions are calculated for this system by solving the time-independent radial Schrödinger equation, which is written as

$$\left[-\frac{1}{2}\frac{d^2}{dr^2} + \frac{l\left(l+1\right)}{2r^2} - \frac{1}{r}\cos\left(r/\lambda_D\right) e^{-r/\lambda_D} \right] U_{nl}\left(r\right) = E_{nl} U_{nl}\left(r\right), \quad (3)$$

where $U_{nl}(r) = r R_{nl}(r)$, with $R_{nl}(r)$ being the radial wave function. Equation (3) is solved over the closed interval $[0,r_0]$ ensuring that wave functions vanish at the boundaries. The solution of Eq. (3) in terms of a finite basis set of Bernstein polynomials (B polynomials) is expressed as

$$U_{nl}\left(r\right) = \sum_{i=0}^{n} c_i B_{i,n}\left(r\right), \quad (4)$$

where the c_i are coefficients of expansion and $B_{i,n}(r)$ are B polynomials of degree n defined over an interval $[a,b]$ as [20–24]

$$B_{i,n}\left(r\right) = C_i^n \frac{\left(r-a\right)^i \left(b-r\right)^{n-i}}{\left(b-a\right)^n}, \quad (5)$$

*shalini_lumb@hotmail.com

†Corresponding author: sonia_lumb@hotmail.com

‡vprasad@ss.du.ac.in

TABLE I. Energy levels calculated for different Debye screening lengths (λ_D) and confinement radii (r_0) values. The data are reported in atomic units. We estimate the maximum uncertainty of our present calculations to be about 1×10^{-6} a.u.

λ_D	r_0	E_{1s}	E_{2s}	E_{2p}	E_{3s}	E_{3p}	E_{3d}	E_{4s}	E_{4p}	E_{4d}	E_{4f}
1	2	0.708 18	4.115 20	2.333 70	10.102 48	7.046 82	4.047 85	18.605 23	14.294 29	10.074 24	6.038 27
	5	0.133 51	0.613 35	0.413 82	1.538 78	1.173 83	0.676 42	2.874 79	2.313 85	1.661 56	0.987 09
	10	0.041 26	0.160 83	0.102 13	0.375 91	0.302 97	0.166 41	0.699 71	0.597 28	0.416 68	0.244 17
	50	0.001 91	0.007 64	0.004 04	0.017 17	0.011 94	0.006 64	0.030 47	0.023 79	0.016 54	0.009 77
2	2	0.347 58	3.789 05	2.033 94	9.775 66	6.729 00	3.777 61	18.277 71	13.971 40	9.771 02	5.786 91
	5	−0.064 97	0.488 38	0.357 28	1.408 83	1.062 97	0.649 79	2.741 06	2.188 65	1.583 97	0.973 96
	10	−0.077 50	0.097 67	0.105 54	0.317 56	0.285 73	0.172 08	0.641 26	0.558 00	0.416 97	0.249 36
	50	−0.077 68	0.002 29	0.004 04	0.009 12	0.011 99	0.006 64	0.020 46	0.023 97	0.016 55	0.009 77
5	2	0.072 92	3.524 44	1.772 73	9.511 06	6.465 81	3.523 55	18.013 01	13.707 44	9.510 71	5.537 68
	5	−0.302 18	0.324 56	0.192 52	1.237 01	0.891 65	0.509 95	2.566 48	2.014 61	1.422 55	0.847 82
	10	−0.306 33	0.044 65	0.045 87	0.243 72	0.203 39	0.141 80	0.559 55	0.471 63	0.355 55	0.229 85
	50	−0.306 33	0.002 45	0.004 21	0.008 39	0.012 41	0.006 70	0.017 02	0.021 90	0.017 11	0.009 77
10	2	−0.025 28	3.427 10	1.675 58	9.413 73	6.368 57	3.426 98	17.915 68	13.610 16	9.413 69	5.441 50
	5	−0.397 22	0.238 76	0.105 39	1.150 77	0.805 30	0.426 27	2.479 93	1.928 03	1.337 08	0.766 20
	10	−0.400 88	−0.019 85	−0.024 42	0.182 68	0.140 83	0.084 14	0.496 80	0.407 92	0.293 96	0.177 85
	50	−0.400 88	−0.034 94	−0.032 47	0.004 16	0.005 42	0.007 75	0.011 36	0.012 72	0.016 13	0.010 77
20	2	−0.075 04	3.377 46	1.625 96	9.364 10	6.318 95	3.377 44	17.866 04	13.560 53	9.364 09	5.392 02
	5	−0.446 52	0.190 91	0.057 30	1.102 88	0.757 39	0.378 73	2.432 00	1.880 10	1.289 30	0.719 01
	10	−0.450 12	−0.063 83	−0.069 65	0.140 10	0.097 93	0.041 62	0.453 89	0.364 83	0.251 16	0.136 69
	50	−0.450 12	−0.076 45	−0.076 06	−0.011 57	−0.010 93	−0.009 55	0.004 20	0.004 70	0.005 82	0.007 85
30	2	−0.091 68	3.360 83	1.609 34	9.347 47	6.302 32	3.360 82	17.849 41	13.543 90	9.347 47	5.375 40
	5	−0.463 12	0.174 48	0.040 84	1.086 45	0.740 95	0.362 33	2.415 56	1.863 66	1.272 88	0.702 65
	10	−0.466 70	−0.079 79	−0.085 77	0.124 34	0.082 13	0.025 84	0.438 09	0.349 00	0.235 37	0.121 09
	50	−0.466 71	−0.092 12	−0.092 00	−0.024 20	−0.023 97	−0.023 49	−0.003 02	−0.002 76	−0.002 20	−0.001 25
40	2	−0.100 00	3.352 50	1.601 01	9.339 14	6.294 00	3.352 50	17.841 09	13.535 58	9.339 14	5.367 08
	5	−0.471 43	0.166 21	0.032 56	1.078 18	0.732 68	0.354 07	2.407 28	1.855 38	1.264 60	0.694 39
	10	−0.475 01	−0.087 94	−0.093 97	0.116 24	0.074 02	0.017 73	0.429 98	0.340 89	0.227 27	0.113 03
	50	−0.475 02	−0.100 20	−0.100 14	−0.031 44	−0.031 33	−0.031 12	−0.008 58	−0.008 45	−0.008 18	−0.007 72
50	2	−0.105 00	3.347 51	1.596 02	9.334 15	6.289 00	3.347 50	17.836 09	13.530 58	9.334 15	5.362 09
	5	−0.476 42	0.161 23	0.027 57	1.073 20	0.727 70	0.349 09	2.402 30	1.850 40	1.259 63	0.689 42
	10	−0.480 01	−0.092 88	−0.098 91	0.111 33	0.069 10	0.012 82	0.425 06	0.335 97	0.222 35	0.108 13
	50	−0.480 01	−0.105 10	−0.105 07	−0.036 03	−0.035 97	−0.035 85	−0.012 50	−0.012 43	−0.012 28	−0.012 03
200	2	−0.120 00	3.332 51	1.581 02	9.319 15	6.274 00	3.332 51	17.821 09	13.515 58	9.319 15	5.347 09
	5	−0.491 42	0.146 25	0.012 59	1.058 22	0.712 72	0.334 12	2.387 32	1.835 42	1.244 65	0.674 45
	10	−0.495 00	−0.107 81	−0.113 86	0.096 42	0.054 19	−0.002 09	0.410 15	0.321 05	0.207 44	0.093 24
	50	−0.495 00	−0.120 00	−0.120 00	−0.050 56	−0.050 56	−0.050 56	−0.026 23	−0.026 24	−0.026 25	−0.026 26

for $i = 0,1,\ldots,n$, where C_i^n are the binomial coefficients given by

$$C_i^n = \frac{n!}{i!\,(n-i)!}. \tag{6}$$

Substituting Eq. (4) into Eq. (3) and taking the scalar product with the B polynomial, $B_{j,n}(r)$, the radial Schrödinger equation is reduced to a symmetric generalized eigenvalue equation of the form

$$(A + F + G)\,C = EDC, \tag{7}$$

where matrix elements $a_{i,j}$, $f_{i,j}$, $g_{i,j}$, and $d_{i,j}$ are defined as

$$a_{i,j} = \frac{1}{2}(B'_{i,n}, B'_{j,n}), \quad f_{i,j} = \frac{l\,(l+1)}{2}\left(\frac{B_{i,n}}{r^2}, B_{j,n}\right),$$

$$g_{i,j} = -\left(\frac{B_{i,n}}{r}\cos\left(r/\lambda_D\right)e^{-r/\lambda_D},\ B_{j,n}\right), \quad d_{i,j} = (B_{i,n}, B_{j,n}). \tag{8}$$

The standard Fortran EISPACK library is used to solve the generalized eigenvalue problem given by Eq. (7) [20,22–24]. The eigenvalues represent energy levels of the system and eigenvectors are used to calculate the corresponding radial wave functions using Eq. (4). The complete wave functions corresponding to H_0 are calculated as

$$\phi_{nlm}(\vec{r}) = R_{nl}(r)\,Y_{lm}(\theta,\varphi), \tag{9}$$

where $Y_{lm}(\theta,\varphi)$ are usual spherical harmonics.

In order to study response of the system to intense short laser pulses, we solve the time-dependent Schrödinger equation written in the form

$$i\frac{\partial\psi}{\partial t} = [H_0 - V(t)]\,\psi, \tag{10}$$

with H_0 being defined by Eq. (1) and

$$V(t) = r\,E_0\cos(\omega_0 t)\,f(t)\cos(\theta), \tag{11}$$

TABLE II. Comparison of energy levels calculated for different Debye screening lengths (λ_D) and confinement radius $r_0 = 50$ a.u. with available results. The data are reported in atomic units. We estimate the maximum uncertainty of our present calculations to be about 1×10^{-6} a.u.

λ_D	E_{1s}	E_{2s}	E_{2p}	E_{3s}	E_{3p}	E_{3d}
7	−0.359 598 325[a]	−0.008 554 215 05[a]	−0.002 829 139 94[a]			
	−0.359 59	−0.008 55	−0.002 82	0.003 83	0.004 97	0.007 00
10	−0.400 878 5[b]	−0.032 673 3[b]				
		−0.034 967 64[c]				
	−0.400 87	−0.034 94	−0.032 46	0.004 16	0.005 41	0.007 75
12.5	−0.420 461 7[b]	−0.050 357 6[b]	−0.048 993 9[b]			
		−0.050 392 22[c]				
	−0.420 46	−0.050 38	−0.048 99	0.002 38	0.003 89	0.007 09
20	−0.450 117 2[b]	−0.076 432 6[b]		−0.011 952 3[b]	−0.011 111 7[b]	−0.009 694 0[b]
		−0.076 449 71[c]				
	−0.450 12	−0.076 44	−0.076 05	−0.011 57	−0.010 92	−0.009 55
25	−0.460 060 8[b]	−0.085 762 1[b]	−0.085 552 0[b]	−0.018 858 6[b]	−0.018 450 5[b]	−0.017 691 0[b]
		−0.085 768 99[c]				
	−0.460 06	−0.085 76	−0.085 55	−0.018 82	−0.018 45	−0.017 68
50	−0.480 007 8[b]	−0.105 103 3[b]	−0.105 074 4[b]	−0.036 021 3[b]	−0.035 964 0[b]	−0.035 849 0[b]
		−0.105 103 59[c]				
	−0.480 00	−0.105 10	−0.105 07	−0.036 02	−0.035 96	−0.035 85
100	−0.490 000 9[b]	−0.115 013 4[b]				
		−0.115 013 46[c]				
	−0.490 00	−0.115 01	−0.115 00	−0.045 61	−0.045 61	−0.045 59

[a]Reference [15].
[b]Reference [7].
[c]Reference [8].

where E_0 is the pulse strength, ω_0 is the laser frequency, θ is the angle between the direction of polarization of the laser pulse and $\hat{r}$, and $f(t)$ is the envelope of the pulse which governs its shape. Equation (10) is solved for two different pulse shapes, viz., $\sin^2$ and square which are defined as

$$f(t) = \begin{cases} \sin^2(\pi t/t_p), & 0 \leqslant t \leqslant tp \\ 0 & \text{otherwise,} \end{cases} \tag{12}$$

and

$$f(t) = \begin{cases} 1, & 0 \leqslant t \leqslant tp \\ 0 & \text{otherwise,} \end{cases} \tag{13}$$

respectively, with t_p being the duration of the laser pulse. The wave function satisfying Eq. (10) can be written as [19,25,26]

$$\psi(\vec{r},t) = \sum_n c_n(t)\, e^{-iE_n t} \phi_n(\vec{r}), \tag{14}$$

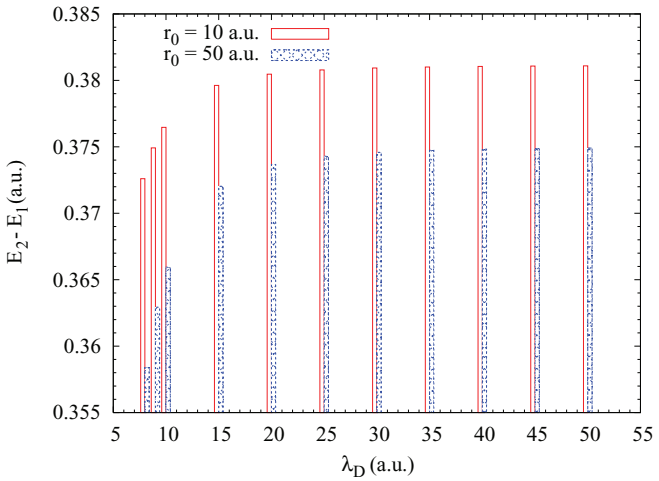

FIG. 1. (Color online) Bar diagram: Energy difference of first two states with respect to Debye screening length λ_D for $r_0 = 10$ and 50 a.u.

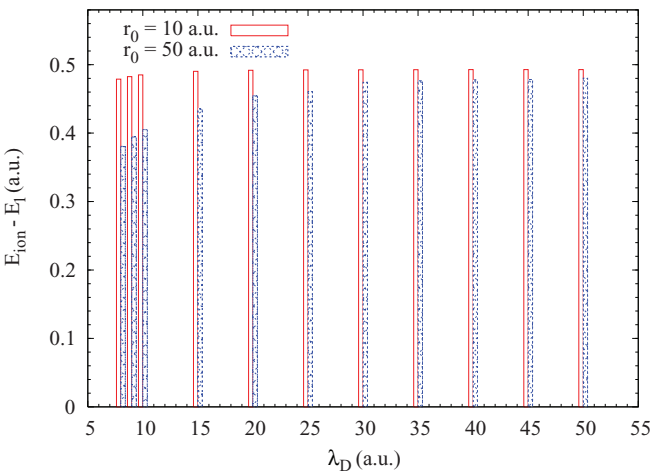

FIG. 2. (Color online) Bar diagram: Energy difference of ground and first-ionized state with respect to Debye screening length λ_D for $r_0 = 10$ and 50 a.u.

TABLE III. Radial dipole matrix elements. The data are reported in atomic units. We estimate the maximum uncertainty of our present calculations to be about 1×10^{-4} a.u.

$\lambda_D = 10$	$r_0 = 10$									
$_{nl}\backslash^{n'l'}$	1 0	2 0	2 1	3 0	3 1	3 2	4 0	4 1	4 2	4 3
1 0	1.503 61	0.632 40	1.382 94	0.444 14	0.858 56	0.836 17	0.294 19	0.499 06	0.967 43	0.563 59
2 0	0.632 40	5.082 79	4.464 97	1.669 71	2.986 41	5.341 23	0.222 70	0.424 99	0.521 34	5.320 05
2 1	1.382 94	4.464 97	4.429 48	0.775 32	1.663 26	4.715 00	0.005 13	0.197 91	0.423 12	4.475 09
3 0	0.444 14	1.669 71	0.775 32	5.619 68	5.085 09	2.800 05	1.853 74	3.391 53	5.357 63	3.969 36
3 1	0.858 56	2.986 41	1.663 26	5.085 09	5.474 33	3.830 66	0.804 50	1.844 71	4.632 09	4.822 09
3 2	0.836 17	5.341 23	4.715 00	2.800 05	3.830 66	5.899 64	0.216 34	0.456 21	1.518 99	6.090 41
4 0	0.294 19	0.222 70	0.005 13	1.853 74	0.804 50	0.216 34	5.409 93	4.793 67	2.601 19	0.746 19
4 1	0.499 06	0.424 99	0.197 91	3.391 53	1.844 71	0.456 21	4.793 67	5.327 52	3.851 51	1.279 17
4 2	0.967 43	0.521 34	0.423 12	5.357 63	4.632 09	1.518 99	2.601 19	3.851 51	5.607 16	2.776 66
4 3	0.563 59	5.320 05	4.475 09	3.969 36	4.822 09	6.090 41	0.746 19	1.279 17	2.776 66	6.568 61
$\lambda_D = 10$	$r_0 = 50$									
1 0	1.503 60	0.532 60	1.238 62	0.072 72	0.122 68	0.025 42	0.144 33	0.298 92	0.130 02	0.002 03
2 0	0.532 60	6.445 06	5.636 01	0.868 62	1.056 55	1.149 75	1.435 58	2.175 36	3.866 46	0.458 43
2 1	1.238 62	5.636 01	5.386 03	0.523 97	0.670 71	0.880 18	0.838 93	1.358 03	3.032 42	0.338 02
3 0	0.072 72	0.868 62	0.523 97	29.316 80	29.831 74	30.366 73	8.220 03	6.098 96	1.730 08	30.192 06
3 1	0.122 68	1.056 55	0.670 71	29.831 74	30.519 72	31.367 64	10.222 73	8.005 79	3.445 23	31.484 00
3 2	0.025 42	1.149 75	0.880 18	30.366 73	31.367 64	32.853 30	14.185 66	11.889 05	7.026 86	33.586 27
4 0	0.144 33	1.435 58	0.838 93	8.220 03	10.222 73	14.185 66	26.434 70	25.708 55	23.735 91	18.195 90
4 1	0.298 92	2.175 36	1.358 03	6.098 96	8.005 79	11.889 05	25.708 55	25.267 35	23.811 84	15.950 06
4 2	0.130 02	3.866 46	3.032 42	1.730 08	3.445 23	7.026 86	23.735 91	23.811 84	23.778 26	11.165 34
4 3	0.002 03	0.458 43	0.338 02	30.192 06	31.484 00	33.586 27	18.195 90	15.950 06	11.165 34	35.047 79
$\lambda_D = 200$	$r_0 = 10$									
1 0	1.499 94	0.633 75	1.391 56	0.437 60	0.839 74	0.842 47	0.291 41	0.491 64	0.960 08	0.564 37
2 0	0.633 75	5.025 78	4.391 28	1.660 99	2.993 15	5.284 12	0.235 85	0.442 03	0.518 79	5.260 19
2 1	1.391 56	4.391 28	4.359 65	0.746 27	1.643 31	4.641 31	0.013 54	0.213 80	0.442 93	4.389 90
3 0	0.437 60	1.660 99	0.746 27	5.631 81	5.093 15	2.798 55	1.852 12	3.399 99	5.368 38	3.995 00
3 1	0.839 74	2.993 15	1.643 31	5.093 15	5.487 84	3.842 51	0.793 97	1.842 05	4.630 17	4.853 37
3 2	0.842 47	5.284 12	4.641 31	2.798 55	3.842 51	5.847 07	0.202 37	0.443 57	1.521 52	6.040 46
4 0	0.291 41	0.235 85	0.013 54	1.852 12	0.793 97	0.202 37	5.420 18	4.802 40	2.606 10	0.743 64
4 1	0.491 64	0.442 03	0.213 80	3.399 99	1.842 05	0.443 57	4.802 40	5.340 99	3.868 02	1.287 58
4 2	0.960 08	0.518 79	0.442 93	5.368 38	4.630 17	1.521 52	2.606 10	3.868 02	5.616 65	2.808 47
4 3	0.564 37	5.260 19	4.389 90	3.995 00	4.853 37	6.040 46	0.743 64	1.287 58	2.808 47	6.534 53
$\lambda_D = 200$	$r_0 = 50$									
1 0	1.499 97	0.558 70	1.290 25	0.243 54	0.516 63	0.385 06	0.148 58	0.306 30	0.264 51	0.066 48
2 0	0.558 70	6.000 08	5.196 23	1.851 02	3.064 65	5.939 22	0.792 07	1.289 30	1.855 99	3.079 35
2 1	1.290 25	5.196 23	5.000 06	0.938 38	1.769 39	4.747 82	0.385 09	0.744 38	1.714 49	2.262 72
3 0	0.243 54	1.851 02	0.938 38	13.501 62	12.729 53	9.488 46	3.821 45	5.493 04	9.549 57	13.781 88
3 1	0.516 63	3.064 65	1.769 39	12.729 53	12.501 51	10.063 77	2.457 46	3.777 72	7.582 47	12.874 91
3 2	0.385 06	5.939 22	4.747 82	9.488 46	10.063 77	10.501 13	0.704 30	1.307 96	3.391 35	10.236 69
4 0	0.148 58	0.792 07	0.385 09	3.821 45	2.457 46	0.704 30	23.773 97	23.039 90	19.982 94	12.613 79
4 1	0.306 30	1.289 30	0.744 38	5.493 04	3.777 72	1.307 96	23.039 90	22.825 93	20.658 38	13.689 79
4 2	0.264 51	1.855 99	1.714 49	9.549 57	7.582 47	3.391 35	19.982 94	20.658 38	20.906 96	15.828 95
4 3	0.066 48	3.079 35	2.262 72	13.781 88	12.874 91	10.236 69	12.613 79	13.689 79	15.828 95	17.976 86

where $\phi_n(\vec{r})$ are the orthogonal eigenstates of H_0 given by Eq. (9) and $c_n(t)$ are time-dependent probability amplitudes. The use of Eq. (14) reduces Eq. (10) to a set of coupled differential equations involving transition dipole matrix elements defined as

$$V_{km} = (\phi_k, V(t)\phi_m). \tag{15}$$

The wave functions given by Eq. (9) are used to calculate these matrix elements for various combinations of initial and final states, and the set of differential equations is solved by the standard fourth-order Runge–Kutta method. These dipole matrix elements may be either zero or nonzero according to the selection rules which depend on the external field and polarization of the applied laser pulse.

The occupation probability of the nth state is given by

$$P_n(t) = |c_n(t)|^2, \tag{16}$$

and the ionization probability is calculated as

$$P_{\text{ion}}(t) = 1 - \sum_m |c_m(t)|^2, \tag{17}$$

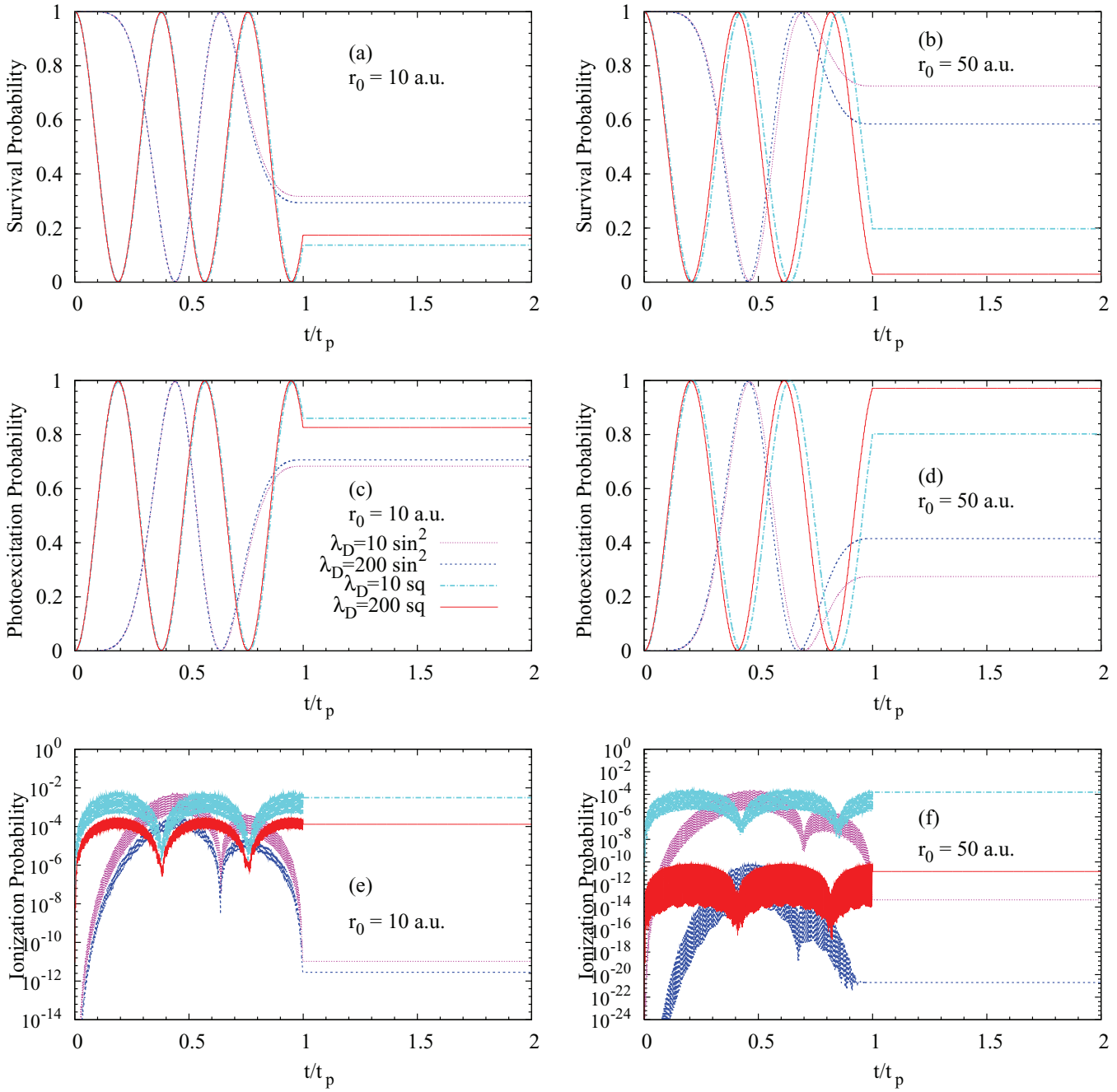

FIG. 3. (Color online) Time variation of various probabilities. The probabilities in panels (e) and (f) are plotted on a logarithmic scale. The legend in panel (c) applies to all panels and r_0 values are as mentioned in respective panels. Laser parameters are $E_0 = 0.01$ a.u., $\omega_0 = E_{2p} - E_{1s}$ a.u., and $t_p = 2067$ a.u. ($\approx$50 fs).

where c_m are coefficients for states having negative energies. The photoexcitation and ionization probabilities are calculated and studied for two different confinement radii and plasma-potential strengths and also as a function of various laser parameters. The range chosen for each of these parameters for the present study is such that it corresponds to experimentally feasible pulses. It may be stated that the laser intensities, wavelengths, and pulse duration used for experimental studies [27,28] fall well within the range of parameters considered by us.

III. RESULTS AND DISCUSSION

We consider a confined hydrogen atom embedded in a plasma environment characterized by ECSCP. The first few energy levels calculated for such a system for various values of confinement radii r_0 and Debye screening length λ_D are given in Table I. The confinement effects are self-evident. The energy spectra is found to consist of both negative- and positive-energy states. The negative-energy states are considered to be bound states while positive-energy states are

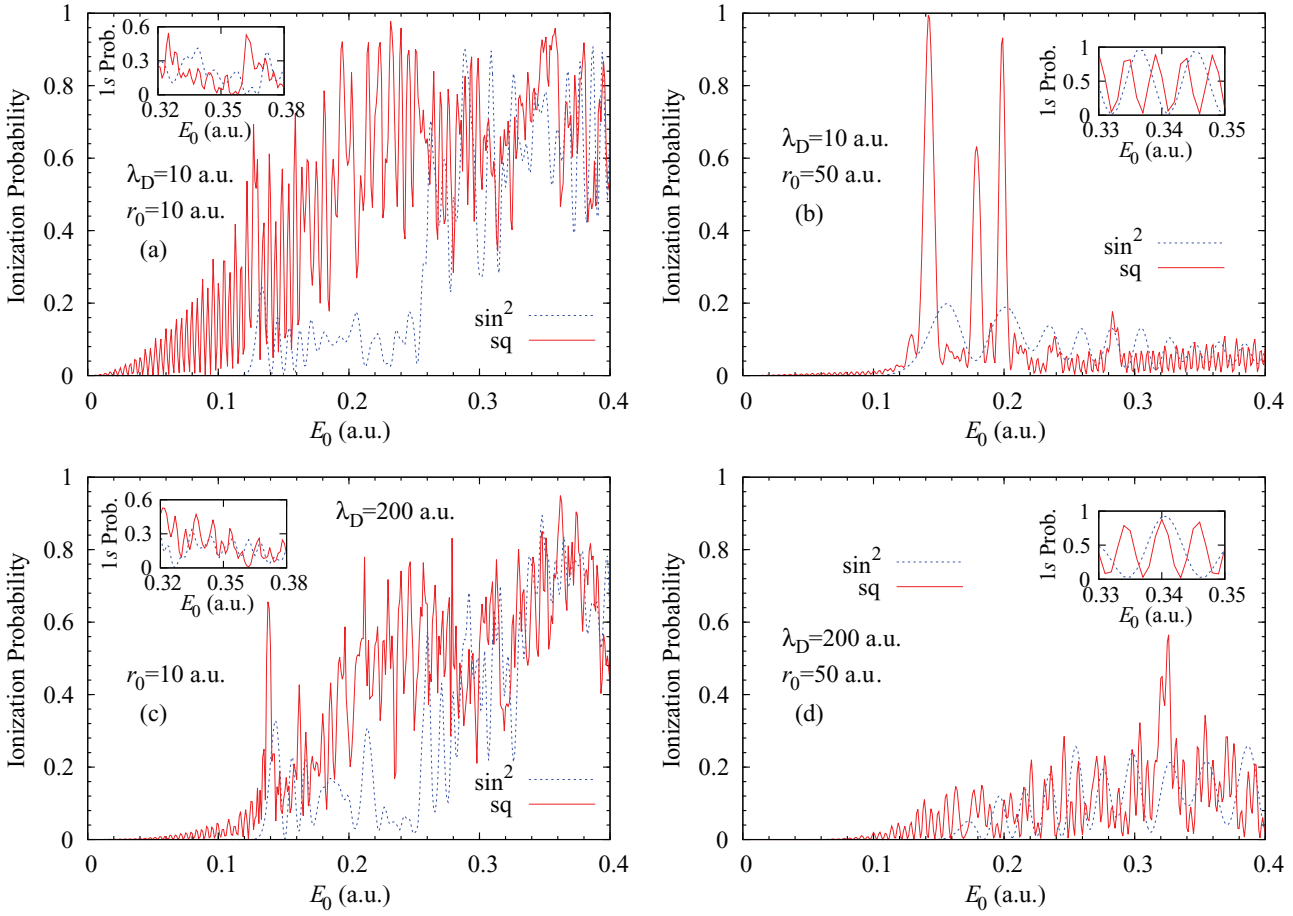

FIG. 4. (Color online) Variation of ionization probabilities with respect to E_0 for sin^2 and square pulses. r_0 and λ_D are as mentioned in each panel. Other laser parameters are $\omega_0 = E_{2p} - E_{1s}$ a.u. and $t_p = 2067$ a.u. The insets show the corresponding variation of survival probability for a small range of E_0 values.

taken as unbound ionized states forming a pseudocontinuum. It is pertinent to mention that photoexcitation refers to transition to any of the bound states whereas ionization means transition to the pseudocontinuum. Because $r_0 = 50$ a.u. corresponds to a loosely bound system, this case closely approximates an unbound hydrogen atom in ECSCP, the results for which are available in the literature [7,8,15]. The energy levels for this case are hence compared with available results for a few λ_D values in Table II which reassures our results.

The changes in wave functions and energy structure due to confinement leading to a change in dipole matrix elements modify the response of the system to external fields. These matrix elements, which play a key role in determining important properties of atomic systems like oscillator strengths, have been calculated using Eq. (15) in order to determine the dynamics of the system due to its interaction with short laser pulses. Table III presents the radial part of the dipole matrix elements for two different spherical confinements and Debye screening lengths. It may be mentioned that these elements are purely a function of wave functions of the system.

Figure 1 depicts how the energy difference between the ground and first-excited state changes with λ_D for $r_0 = 10$ and 50 a.u. As the screening of the Coulomb potential increases, this difference gradually decreases and suffers a sharp fall for smaller λ_D. This effect is less prominent in case of $r_0 = 10$ a.u., which may be attributed to a change in the energy structure due to confinement. A plot of the difference between energies of the ground and first-ionized state with respect to λ_D in Fig. 2 exhibits similar features. At a particular value of λ_D, called the critical Debye screening length, a given energy level no longer remains bound and hence a transition to this quasibound state would also correspond to ionization. The case $r_0 = 50$ a.u., which closely approximates a free hydrogen atom, has a large number of bound states but if plasma confinement is introduced, the number of bound states decreases with decrease in λ_D along with the shifting of levels. Hence, with decreasing λ_D, ionization may occur by transition to relatively lower energy levels, and this causes the observed fall in energy difference. On the other hand, for $r_0 = 10$ a.u., the number of bound states remains three for the entire range of λ_D considered in Fig. 2. The decrease of relative energy with λ_D in this case is only due to the shifting of energy levels. These results along with the data in Tables I and III would prove useful in interpreting the response of the system to laser pulses.

The system is exposed to a short intense laser pulse of femtosecond range and the effect of varying the Debye screening length and confinement radius on its dynamics is explored. Time variation of survival, photoexcitation, and

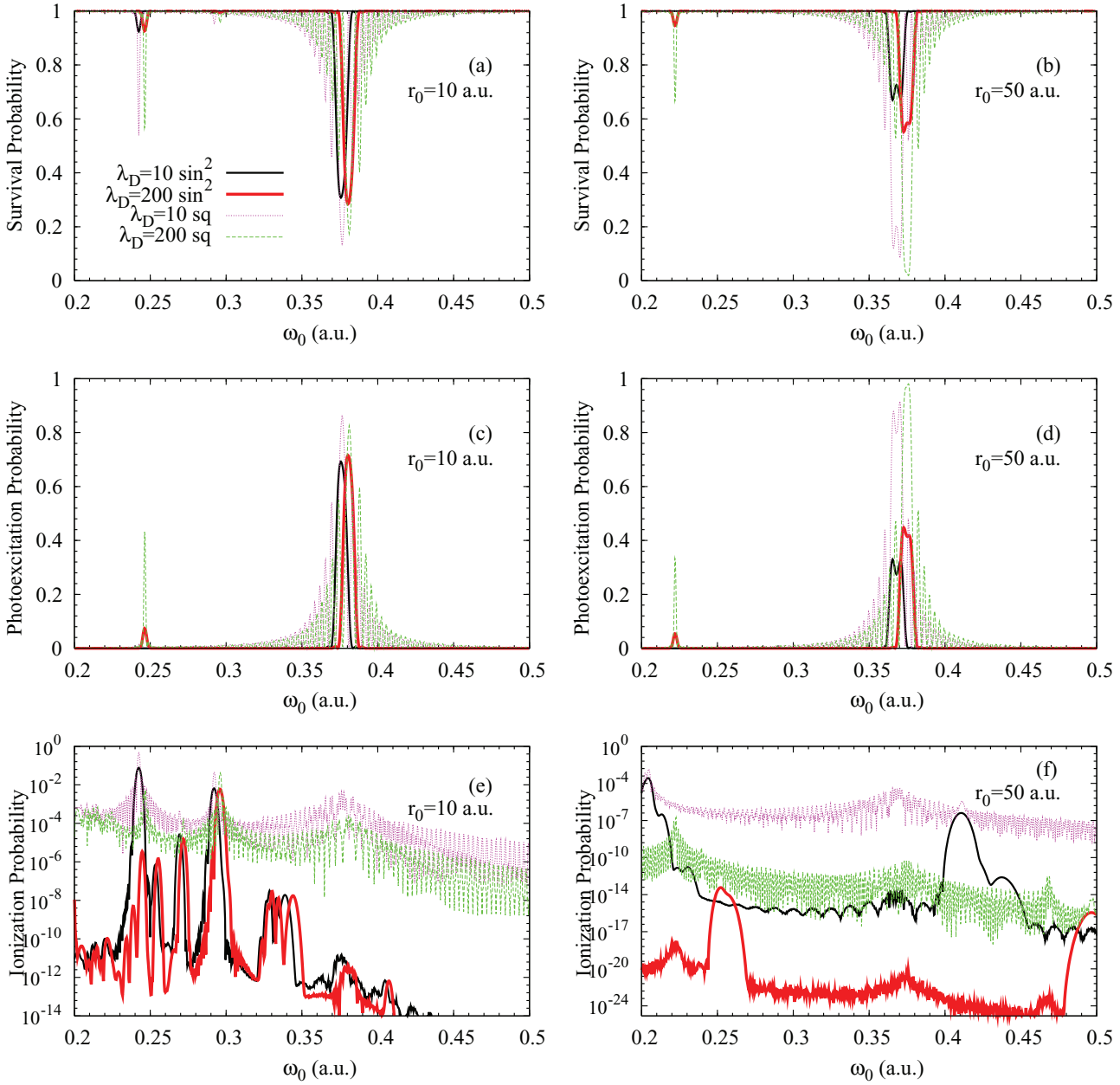

FIG. 5. (Color online) Variation of various probabilities with respect to w_0 for r_0 values as mentioned in respective panels. The probabilities in panels (e) and (f) are plotted on a logarithmic scale. The legend in panel (a) applies to all panels. Other laser parameters are $E_0 = 0.01$ a.u. and $t_p = 2067$ a.u.

ionization probabilities are calculated and studied under the dipole approximation and the results are presented in Fig. 3 for pulse strength $E_0 = 0.01$ a.u. (intensity $\approx 3.51 \times 10^{12}$ W/cm^2), duration $t_p = 2067$ a.u. (≈ 50 fs), frequency $w_0 = E_{2p} - E_{1s}$ a.u., and two strengths of plasma potential, viz., $\lambda_D = 10$ and 200 a.u. Figures 3(a) and 3(b) show survival, 3(c) and 3(d) show photoexcitation, and 3(e) and 3(f) show ionization probabilities for $r_0 = 10$ and 50 a.u., respectively. Note that Figs. 3(e) and 3(f) show ionization probability in logarithmic scale since ionization is very weak which implies that a pulse strength of 0.01 a.u. is not enough to produce sufficient ionization.

The probabilities oscillate until the pulse dies out after which the system stabilizes and they attain constant values. Figures 3(c)–3(f) show that photoexcitation and ionization probabilities are more in the case of square-shaped pulses for both values of λ_D and r_0 and correspondingly the survival probability in Figs. 3(a) and 3(b) diminishes. This is as expected because of the sharp edge of and larger area under a square-shaped pulse in comparison to a $\sin^2$ pulse, which imparts more fluence to the system. Figures 3(e) and 3(f) clearly demonstrate the fact that ionization is much more probable for heavily screened and tightly bound systems. This effect of λ_D and r_0 is attributed to changes in energy levels, wave functions, dipole matrix elements, and oscillator strengths.

The end-of-pulse behavior is studied as a function of laser parameters like pulse strength E_0, frequency ω_0, and duration

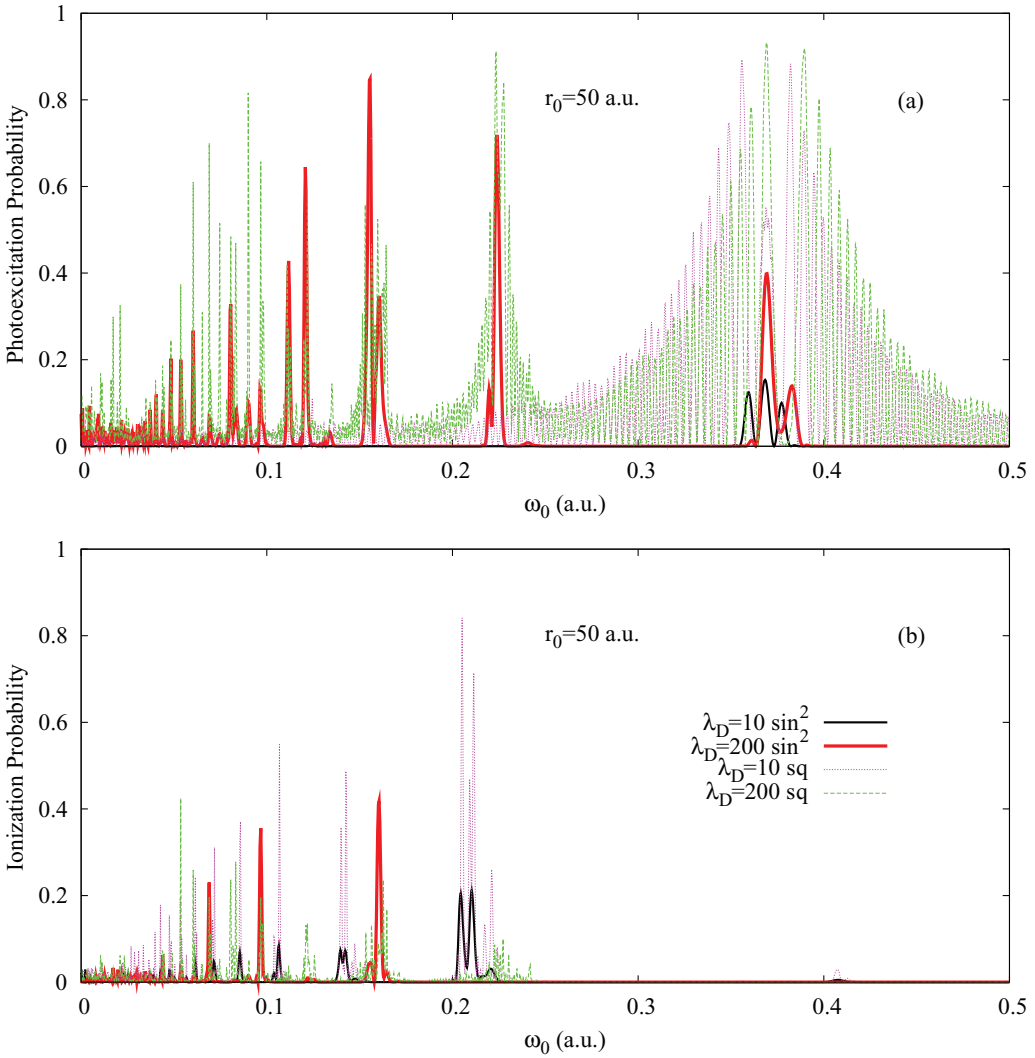

FIG. 6. (Color online) Variation of transition probabilities with respect to w_0 for $r_0 = 50$ a.u. The legend in panel (b) applies to both panels. Other laser parameters are $E_0 = 0.05$ a.u. and $t_p = 2067$ a.u.

t_p by varying only one of these at a time. Figure 4 shows the effect of changing pulse strength E_0 on ionization probabilities for $\sin^2$ and square-shaped pulses for two different values of r_0 and λ_D, as mentioned in the figure panels. The laser frequency ω_0 is taken as $E_{2p} - E_{1s}$ a.u. and the duration t_p is 2067 a.u. The insets to Fig. 4 show the corresponding behavior of the survival probability for a small selected range of E_0 values. The ionization probability in Fig. 4(b) and 4(d) has been multiplied by a factor of two in order to make it appreciably visible. It is inferred that ionization is much more probable for the case of a square pulse as compared to a $\sin^2$ pulse. The insets show complete depopulation of the ground state for some E_0. In general, the ionization probability is greater for smaller λ_D and r_0. Also, the threshold value of E_0 for achieving ionization decreases due to Coulomb screening and spherical confinement.

Figure 5 exhibits survival, excitation, and ionization probabilities as a function of laser frequency ω_0. E_0 is taken as 0.01 a.u and t_p is 2067 a.u. The probabilities in Figs. 5(e) and 5(f) are plotted on a logarithmic scale. Probability flows from $1s$ to excited states at resonance. Even complete depopulation occurs, as seen in Fig. 5(b) for $r_0 = 50$ a.u. and $\lambda_D = 200$ a.u. for the case of square pulse. The dynamics of a system is strongly dependent on the shape of the applied pulse and gives rise to interesting effects. In the case of a $\sin^2$ pulse there is a smooth transfer of energy to a system leading to well-defined resonance peaks. On the other hand, the sharp rise and fall of a square pulse leads to a sudden transfer of energy which is responsible for the observed pattern of multiresonance. Redshifting of resonance peaks with increased Debye screening or decreased confinement is due to changes in the energy spectrum. The ionization probability is very small, as seen in Figs. 5(e) and 5(f). This low-field ionization of the bound hydrogen atom is as expected. It is anticipated that, for relatively high fields, transition probabilities should increase. This fact has been verified by increasing the field to 0.05 a.u., keeping other parameters fixed, which results in enhanced excitation as well as ionization with the broadening of peaks as shown in Fig. 6 for $r_0 = 50$ a.u. It may be noted that, at higher pulse strength, the ac Stark effect [29] also plays an important role in determining the exact resonant frequencies along with increased multiphoton effects.

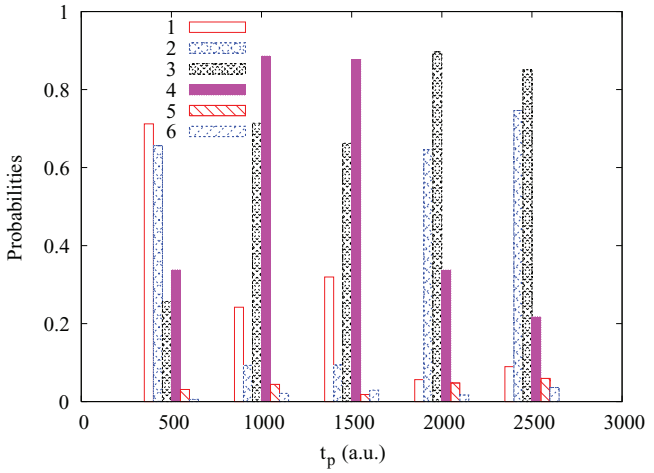

FIG. 7. (Color online) Bar diagram: Variation of various probabilities with respect to duration of the pulse (t_p) for $\sin^2$ and square pulses. Legend 1: $1s$ (square), 2: $1s$ ($\sin^2$), 3: excitation (square), 4: excitation ($\sin^2$), 5: ionization (square), 6: ionization ($\sin^2$). Other parameters are $r_0 = 50$ a.u., $\lambda_D = 10$ a.u., $E_0 = 0.5$ a.u., and $\omega_0 = E_{2p} - E_{1s}$ a.u.

The effect on the dynamics of varying the duration of the laser pulse is also studied. As an example, Fig. 7 shows different probabilities for $\lambda_D = 10$ a.u. and $r_0 = 50$ a.u., $E_0 = 0.5$ a.u., and $\omega_0 = E_{2p} - E_{1s}$ a.u. for both $\sin^2$ and square pulses. For small t_p, both excitation and ionization probabilities are low and survival probability is high. As the pulse becomes broader, the transition probabilities increase with the corresponding decrease in survival probability because the system is exposed to the laser field for a comparatively longer period of time. With further increase in t_p, excitation saturates, survival probability remains low, and ionization gradually increases. For higher t_p, the pattern followed may be explained by taking into account the fact that a strong mixing of levels takes place in the presence of broad pulses. This pattern is unlike molecular systems where differences in energy levels are almost constant.

IV. CONCLUSIONS

The energy spectra and radial dipole matrix elements of spherically confined hydrogen atoms embedded in an exponential-cosine-screened Coulomb potential (ECSCP), characterizing a dense plasma environment, are calculated by using the B-polynomial basis-set method. The transition probabilities due to an applied short laser pulse are studied and the effects of varying the pulse strength, frequency, and duration are explored and analyzed. Photoexcitation and ionization probabilities are found to depend significantly on confinement radius and Debye screening length. Two different pulse shapes, viz., $\sin^2$ and square, are considered and interesting results are obtained. As anticipated, pulse shape plays a major role in determining the dynamics of the system.

[1] J. K. Saha, S. Bhattacharyya, T. K. Mukherjee, and P. K. Mukherjee, J. Quant. Spectrosc. Radiat. Transfer **111**, 675 (2010).

[2] S. Kar and Y. K. Ho, Phys. Rev. A **71**, 052503 (2005); **72**, 010703 (2005); **73**, 032502 (2006); **75**, 062509 (2007); **83**, 042506 (2011).

[3] Y. Y. Qi, Y. Wu, and J. G. Wang, Phys. Plasmas **16**, 033507 (2009).

[4] Y. D. Jung, Phys. Fluids B **5**, 3432 (1993).

[5] S. Sahoo and Y. K. Ho, Phys. Plasmas **13**, 063301 (2006).

[6] O. Bayrak and I. Boztosun, Int. J. Quantum Chem., **107**, 1040 (2007).

[7] S. M. Ikhdair and R. Sever, J. Math. Chem. **41**, 329 (2007).

[8] S. Paul and Y. K. Ho, Comput. Phys. Commun. **182**, 130 (2011).

[9] L. U. Ancarani, K. V. Rodriguez, G. Gasaneo, and D. M. Mitnik, J. Phys.: Conf. Ser. **488**, 152015 (2014).

[10] A. Ghoshal and Y. K. Ho, J. Phys. B: At., Mol. Opt. Phys. **42**, 075002 (2009).

[11] S. M. Ikhdair and R. Sever, Z. Phys. D: At., Mol. Clusters **28**, 1 (1993).

[12] A. N. Sil, B. Saha, and P. K. Mukherjee, Int. J. Quantum Chem. **104**, 903 (2005).

[13] A. N. Sil, S. Canuto, and P. K. Mukherjee, Adv. At. Mol. Opt. Phys. **58**, 115 (2009).

[14] S. Paul and Y. K. Ho, Phys. Plasmas **16**, 063302 (2009).

[15] C. Y. Lin and Y. K. Ho, Eur. Phys. J. D **57**, 21 (2010).

[16] P. K. Shukla and B. Eliasson, Phys. Lett. A **372**, 2897 (2008).

[17] S.-C. Na and Y.-D. Jung, Phys. Lett. A **372**, 5605 (2008).

[18] S.-C. Na and Y.-D. Jung, Phys. Scr. **78**, 035502 (2008).

[19] V. Prasad, B. Dahiya, and K. Yamashita, Phys. Scr. **82**, 055302 (2010).

[20] S. Lumb, S. Lumb, and V. Prasad, Indian J. Phys., doi: 10.1007/s12648-014-0519-1.

[21] M. I. Bhatti, Adv. Studies Theor. Phys. **3**, 451 (2009).

[22] M. I. Bhatti and W. F. Perger, J. Phys. B: At., Mol. Opt. Phys. **39**, 553 (2006).

[23] S. Lumb, S. Lumb, and V. Prasad, J. Mod. Phys. **4**, 1139 (2013).

[24] S. Lumb, S. Lumb, and V. Prasad, Quantum Matter **2**, 314 (2013).

[25] S. Barmaki, S. Hennani, and S. Laulan, J. Mod. Phys. **4**, 27 (2013).

[26] S. Laulan, J. Haché, H. S. Ba, and S. Barmaki, J. Mod. Phys. **4**, 20 (2013).

[27] D. B. Milošević, G. G. Paulus, D. Bauer, and W. Becker, J. Phys. B: At., Mol. Opt. Phys. **39**, R203 (2006).

[28] G. G. Paulus, F. Lindner, H. Walther, A. Baltuška, E. Goulielmakis, M. Lezius, and F. Krausz, Phys. Rev. Lett. **91**, 253004 (2003).

[29] B. Sharma, V. Prasad, and M. Mohan, J. Chem. Phys. **89**, 1322 (1988).